Tunneling induced transparency and slow light in quantum dot molecules

H. S. Borges, L. Sanz, J. M. Villas-Bôas, O. O. Diniz Neto, and A. M. Alcalde
Instituto de Física, Universidade Federal de Uberlândia, 38400-902, Uberlândia-MG, Brazil
(Received 10 February 2012; published 20 March 2012)

Electromagnetic induced transparency is an optical phenomenon that allows transmission of a laser beam through a dense medium by using a control laser beam. Here, we propose the use of a quantum molecule where the control laser beam is replaced by the electron tunneling between quantum dots, which can be controlled by an external electric field, opening the possibility to induce transparency and slow light with electric gates. Our results show that a transparency window appears if the tunneling strength T_e and the decay rate of direct exciton Γ_1 obey the condition $T_e/\Gamma_1 \leqslant 0.5$.

DOI: 10.1103/PhysRevB.85.115425 PACS number(s): 73.21.La, 73.40.Gk, 03.65.Yz

I. INTRODUCTION

It is well established that quantum interference between different excitation paths of atomic states pumped by coherent radiation can control its optical response. An example is the suppression of light absorption in a narrow region of frequency which is associated with both, the enhancement of the nonlinear susceptibility and the propagation of an optical pulse at very low group velocities. This physical phenomenon is known as electromagnetically induced transparency (EIT)[1] and requires an atomic system with two ground states optically coupled optically coupled to an excited state by a weak probe and a strong control near-resonant optical fields (Λ system).

Semiconductor nanostructures coherently driven by strong electromagnetic fields have been used to investigate other quantum interference phenomena as Autler-Townes splitting (ATS) and Mollow triplets.[2,3] Some of these effects were partially observed in single quantum dots (QDs). For example, it has been confirmed that under strong optical excitation, the interference between the exciton-biexciton transition produces a dip in the optical absorption line.[4] Also, a coherent absorption dip in pump-probe experiment was observed in a ten layer quantum dot structure and the results show that the dip effect is robust against the effects of temperature and inhomogeneous broadening.[5] Several other works have also studied this effect in quantum wells and QDs systems when two laser beams are applied on the sample.[6–8]

Semiconductor quantum dots coupled by tunneling, also known as quantum dot molecules (QDMs), are systems where it is possible to create a Λ level configurations. In structurally asymmetric artificial molecules, an external electric field allows us to control the tunneling of electrons or holes and create a multilevel structure of excitonic states.[9] The population of these levels can be coherently controlled through an appropriate set of parameters experimentally accessible. Protection of quantum states,[10] excitonic entanglement,[11,12] slow light,[13] and controlled rotation of exciton qubits[14] has been recently proposed in these systems.

In this work, we analyze the linear optical susceptibility of a QDM under coherent excitation and considering the spontaneous exciton decay and pure dephasing as decoherence channels. We numerically solve the Liouville-von Neumman-Lindblad equation in the Markovian approximation and our results show that, in the limit of low optical excitation, the tunneling coupling establishes an efficient destructive quantum interference path that creates a transparency window in the absorption spectra. In the following, we will call this effect *tunneling induced transparency* (TIT) because of the critical role of tunneling in the appearance of transparency in QDMs. By solving numerically the density matrix, we are able to explore a wide range of parameters and we can establish the condition that defines a threshold between transparency and the ATS and map the behavior of group velocity in this system.

The paper is organized as follows: in Sec. II, we discuss the physical system and model. Section III is devoted to the analysis of the properties of optical susceptibility considering the effects of tunneling, decoherence mechanism, and detuning, including a particular discussion about the group velocity. Section IV is reserved for our conclusions.

II. PHYSICAL SYSTEM AND MODEL

In order to investigate the optical response of a vertical aligned quantum dot molecule, we consider a structural asymmetry, which is introduced intentionally in order to inhibit the hole tunneling.[15] The system is driven by an electromagnetic field and a gate electric field is applied along of growth direction to provide a control of the level alignment. As discussed in our previous work,[10,16] the fundamental physics of this system is captured considering a three-level Λ-type Hamiltonian given by

$$H = \sum_{j=0}^{2} E_j |j\rangle\langle j| + T_e|1\rangle\langle 2| + \hbar\Omega \exp(i\omega_L t)|0\rangle\langle 1| + \text{H.c.}, \tag{1}$$

where $E_j = \hbar\omega_j$ is the energy of state $|j\rangle$, T_e the tunneling coupling, ω_L the laser frequency, and $\Omega = \mu_{01}E/2\hbar$ the two-level optical coupling, where μ_{01} is the dipole momentum matrix element and E the electric field amplitude.

A schematic representation of energy levels and their couplings and parameters is given in Fig. 1. In absence of optical excitation, there is no excitons inside both quantum dots, condition represented by the state $|0\rangle$. By applying an electromagnetic field, a direct exciton is created inside the left quantum dot, which corresponds to state $|1\rangle$. The external electric field modifies the band profiles alignment, allowing the electron to tunnel from one QD to another forming the indirect exciton, which we denoted as state $|2\rangle$.

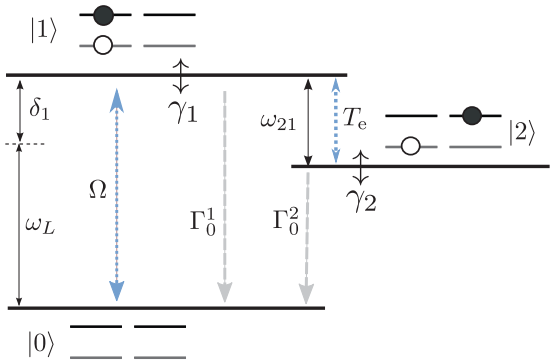

FIG. 1. (Color online) Scheme of energy energy levels, decoherence channels, detunings, and relevant Hamiltonian parameters. See text for details.

The system dynamics is described by Liouville-von Neumman-Lindblad equation:[10]

$$\frac{d\rho}{dt} = -\frac{i}{\hbar}[H,\rho(t)] + L(\rho), \tag{2}$$

being $\rho(t)$ the density matrix operator, H is the three-level system Hamiltonian (1), and $L(\rho)$ represents the Liouville operator that describes the decoherence process. Here, we consider two decoherence mechanisms: the spontaneous decay of excitonic states and the pure dephasing channels. The main source of exciton pure dephasing in QDs is the electron-acoustic phonon interaction.[17] In QDMs, the effects of pure dephasing were experimentally explored by Borri *et al.*,[18] who showed that for QDMs there is an enhancement of the pure dephasing channels, in contrast to QDs, where at low temperatures no pure dephasing occurs.

Assuming the Markovian approximation, the Liouville operator that describes both dissipative processes is given by

$$L(\rho) = \frac{1}{2}\sum_i \Gamma_i^j (2|j\rangle\langle i|\rho|i\rangle\langle j| - \rho|i\rangle\langle i| - |i\rangle\langle i|\rho) + \gamma_i(2|i\rangle\langle i|\rho|i\rangle\langle i| - \rho|i\rangle\langle i| - |i\rangle\langle i|\rho), \tag{3}$$

where the first term describes the spontaneous decay process from the state $|i\rangle$ to the state $|j\rangle$ with rate Γ_i^j and the second term is the pure dephasing with rate γ_i. Using the Eq. (3) in the Liouville-von Neumman-Lindblad equation (2), we obtain the complete set of coupled differential equation for the density matrix ρ_{ij} elements as follows:

$$\dot{\rho}_{00} = -i\Omega(\rho_{10} - \rho_{01}) + \Gamma_0^1\rho_{11} + \Gamma_0^2\rho_{22}, \tag{4a}$$

$$\dot{\rho}_{01} = i[\delta_1\rho_{01} + \Omega(\rho_{00} - \rho_{11}) + T_e\rho_{02}] - (\Gamma_0^1/2 + \gamma_3)\rho_{01}, \tag{4b}$$

$$\dot{\rho}_{02} = i\left[\frac{\rho_{02}}{2}(\delta_1 + \delta_2) - \Omega\rho_{12} + T_e\rho_{01}\right] - \left(\Gamma_0^1/2 + \gamma_4\right)\rho_{02}, \tag{4c}$$

$$\dot{\rho}_{10} = i[-\delta_1\rho_{01} + \Omega(\rho_{11} - \rho_{00}) - T_e\rho_{20}] - \left(\Gamma_0^1/2 + \gamma_3\right)\rho_{10}, \tag{4d}$$

$$\dot{\rho}_{11} = i\left[\Omega(\rho_{10} - \rho_{01}) + T_e(\rho_{12} - \rho_{21})\right] - \Gamma_0^1\rho_{11}, \tag{4e}$$

$$\dot{\rho}_{12} = i\left[\frac{\rho_{12}}{2}(\delta_2 - \delta_1) - \Omega\rho_{02} + T_e(\rho_{11} - \rho_{22})\right] - \left[\left(\Gamma_0^1 + \Gamma_0^2\right)/2 + \gamma_5\right]\rho_{12}, \tag{4f}$$

$$\dot{\rho}_{20} = i\left[-\frac{\rho_{20}}{2}(\delta_1 + \delta_2) + \Omega_{21} - T_e\rho_{10}\right] - \left(\Gamma_0^2/2 + \gamma_4\right)\rho_{20}, \tag{4g}$$

$$\dot{\rho}_{21} = i\left[\frac{\rho_{21}}{2}(\delta_1 - \delta_2) + \Omega\rho_{20} + T_e(\rho_{22} - \rho_{11})\right] - \left[\left(\Gamma_0^1 + \Gamma_0^2\right)/2 + \gamma_5\right]\rho_{21}, \tag{4h}$$

$$\dot{\rho}_{22} = iT_e\left(\rho_{21} - \rho_{12}\right) - \Gamma_0^2\rho_{22}, \tag{4i}$$

where $\gamma_3 = \gamma_1/2$, $\gamma_4 = \gamma_2/2$, and $\gamma_5 = (\gamma_1 + \gamma_2)/2$. The detunings are defined as $\delta_1 = (\omega_{01} - \omega_L)$ and $\delta_2 = \delta_1 + 2\omega_{21}$ with ω_{ij} the transition frequency between $|i\rangle$ and $|j\rangle$ states.

In our model, the laser field only couples the vacuum and direct exciton states $|0\rangle$ and $|1\rangle$, with Rabi frequency Ω. The linear optical susceptibility function $\chi = \chi' + i\chi''$ is a complex function that contains all the information about the coherent optical excitations. For our system, the linear susceptibility is just proportional to the density matrix element ρ_{01}:

$$\chi = \frac{\Gamma_{\text{opt}}}{V}\frac{|\mu_{10}|^2}{\varepsilon_0\hbar\Omega}\rho_{01}, \tag{5}$$

where Γ_{opt} is the optical confinement factor,[13] V is the volume of a single QD, and ε_0 is the dielectric constant. The optical absorption spectrum $\alpha(\omega_L)$ is determined by the imaginary part of the linear susceptibility χ''. In addition, the refraction

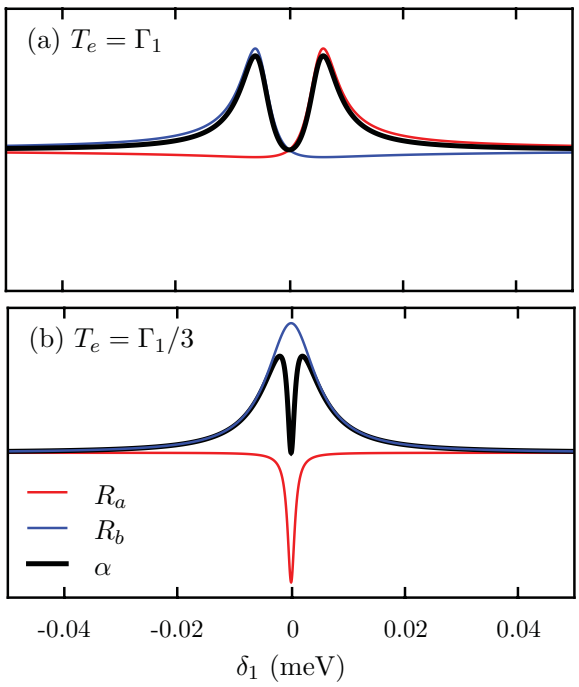

FIG. 2. (Color online) Imaginary part of resonances R_a and R_b and optical absorption α as a function of detuning δ_1 for different T_e/Γ_1 ratios. (a) Autler-Townes splitting regime and (b) tunneling induced transparency regime.

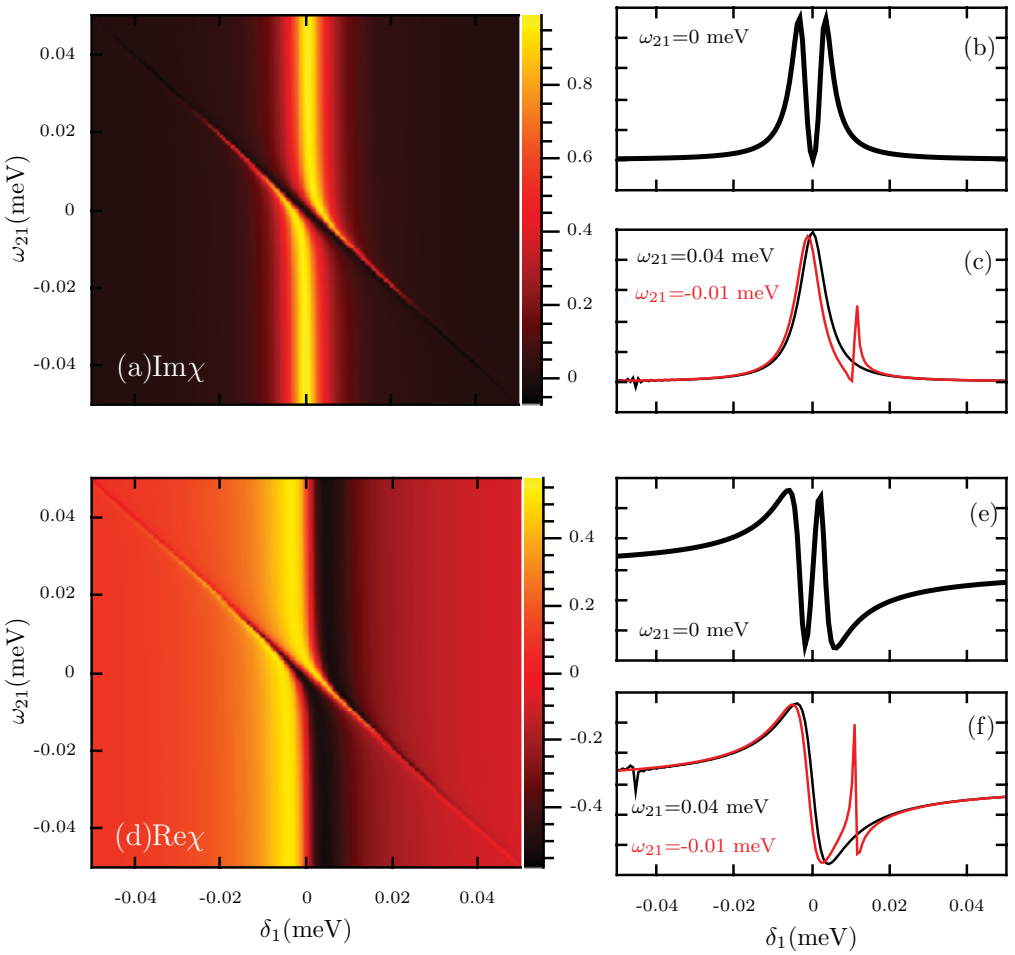

FIG. 3. (Color online) Imaginary (a) and real (d) parts of optical susceptibility as a function of laser detuning δ_1 and ω_{21} within the TIT condition $T_e = \Gamma_1/2$. Absorption profiles as a function of δ_1 for fixed values of ω_{21} are shown for (b) $\omega_{21} = 0$ and (c) $\omega_{21} = -0.01$ meV (red line) and $\omega_{21} = 0.04$ (black line). Real part profiles are shown for (e) $\omega_{21} = 0$ and (f) $\omega_{21} = -0.01$ meV (red line) and $\omega_{21} = 0.04$ (black line).

index is defined in terms of the complex dielectric function as

$$n(\omega_L) = \sqrt{\tfrac{1}{2}[\epsilon'(\omega_L) + \sqrt{\epsilon'(\omega_L) + \epsilon''(\omega_L)}]}, \tag{6}$$

where the real and imaginary parts of ϵ and χ are related by $\epsilon' = 1 + 4\pi\chi'$ and $\epsilon'' = 4\pi\chi''$, respectively. The light group velocity v_g is a function of the refraction index given by

$$v_g/c = \frac{1}{n + \omega_L(dn/d\omega_L)}, \tag{7}$$

where c is the light speed in vacuum. With this considerations, we investigate the behavior of the absorption profile and refractive index of the medium in presence of the coupling tunneling by solving numerically the coupled equations (4) in the steady regime.

III. RESULTS AND DISCUSSION

For our investigation, we consider realistic parameters for InAs self-assembled QDM under coherent laser excitation, which can be summarized as $\hbar\omega_{10} \sim 1.6$ eV,[19,20] $\hbar\Omega \simeq 0.05$–1.0 meV,[21,22] the effective dephasing parameters, $\Gamma_1 = \Gamma_0^1/2 + \gamma_3$ and $\Gamma_2 = \Gamma_0^2/2 + \gamma_4$, are in energy units $\Gamma_1 \sim 2$–10 μeV[18,23,24] and $\Gamma_2 \sim 10^{-3}\Gamma_1$.[25] The tunneling coupling, which depends the barrier characteristics and the external electric field, was selected to be $T_e \sim 0.01$–0.1 meV[26] or $T_e \sim 1$–10 meV,[27] for weak and strong tunneling regime, respectively. Other parameters such as the optical confinement factor $\Gamma_{\rm opt} = 6 \times 10^{-3}$, momentum matrix element $\mu_{10}/e = 21$ Å, and QD volume V, were taken from Ref. 28.

Initially, we investigate the behavior of optical susceptibility and search for transparency windows in our system. It is important to mention that sharp reduction or dips in the optical absorption line can be produced by two type of processes: the TIT and ATS. Transparency is a consequence of the destructive interference produced between two optical paths, observed when the coupling field is weaker than the optical transition decay rate. A second signature of this phenomenon is an abrupt change on the slope of the real part of the susceptibility in the same interval of frequencies where the dip is observed. ATS appears in the opposite limit, when the field coupling is stronger than the decay rate and consists in the splitting of the absorption spectra in two Lorentzian-like peaks separated by a zero absorption gap. Thus the reduction in the absorption can

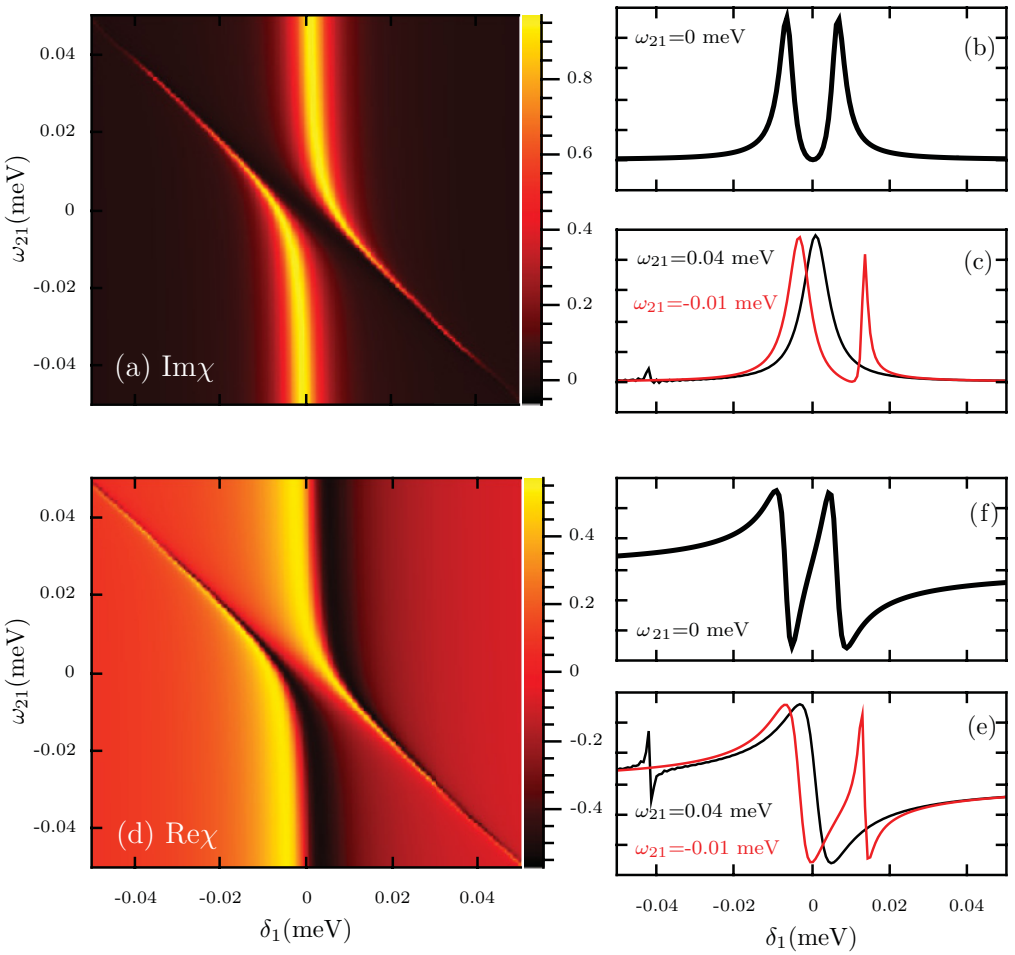

FIG. 4. (Color online) Same as in Fig. 3 for $T_e = \Gamma_1$.

be interpreted either as a process of destructive interference between two competitive optical channels, or as the splitting into two components of the absorption spectra.

In order to establish a specific condition to distinguish TIT from ATS, we solve analytically the set of equations (4) in the limit of of low excitation approximation ($T_e \gg \Omega$) to obtain the density matrix element ρ_{10}:

$$\rho_{10} = \frac{(\delta_1 + \delta_2) + 2i\Gamma_2}{(i\delta_1 - \Gamma_1)[i(\delta_1 + \delta_2) - 2\Gamma_2] + 2T_e^2}, \tag{8}$$

which is a sum of the two components:

$$R_a = \frac{\delta_1^b - i\Gamma_1}{\delta_1^a - \delta_1^b} \frac{1}{(\delta_1 - \delta_1^a)}, \tag{9a}$$

$$R_b = \frac{\delta_1^a - i\Gamma_1}{\delta_1^b - \delta_1^a} \frac{1}{(\delta_1 - \delta_1^b)}, \tag{9b}$$

with

$$\delta_1^{a,b} = \tfrac{1}{2}[-i(\Gamma_2 + \Gamma_1) - \omega_{21} \mp \sqrt{Z}]. \tag{10}$$

Here, the upper (lower) sign correspond to $a(b)$ resonance and the function Z is given by $Z = 4T_e^2 - \Gamma_2^2 + 2\Gamma_2(\Gamma_1 + i\Gamma_2) - \Gamma_1^2 - 2i\omega_{21}\Gamma_1 + \omega_{21}^2$. The threshold value of T_e that separates TIT (weak coupling) from ATS (strong coupling) is obtained from the analysis of resonances[29] $R_{a,b}$. In Fig. 2, we plot the contributions R_a and R_b resonances to total absorption profile as a function of detuning δ_1 considering $\omega_{21} = 0$ (resonant tunneling condition). We use different values of T_e/Γ_1 to illustrate that the evolution of the absorption line from ATS to TIT depends on this ratio. Even at the intermediate coupling regime $T_e = \Gamma_1$, shown in Fig. 2(a), the absorption profile has two separated peaks, each corresponding to resonances R_a and R_b. That means that the dip (black line) can be interpreted as the gap between two different components of absorption, a doublet, which is a characteristic of the ATS effect. In the situation of weak coupling, as shown in Fig. 2(b), the resonances R_a and R_b are strongly overlapped and the overall absorption line is composed by two Lorentzian-like peaks and one of them negative. This behavior reveals a destructive interference process which produces a narrow dip in the absorption profile. For $\omega_{21} = 0$, we obtain the threshold value $T_e = (\Gamma_1 - \Gamma_2)/2$. In our system, the condition $\Gamma_1 \gg \Gamma_2$ is valid, therefore the threshold is given by $T_e/\Gamma_1 = 0.5$.

In Figs. 3 and 4, we show the real and imaginary parts of the optical susceptibility obtained numerically as a function of the detuning parameters δ_1 and ω_{21}. We analyze our results considering the threshold condition $T_e = \Gamma_1/2$, which corresponds to the TIT regime. The imaginary and real parts

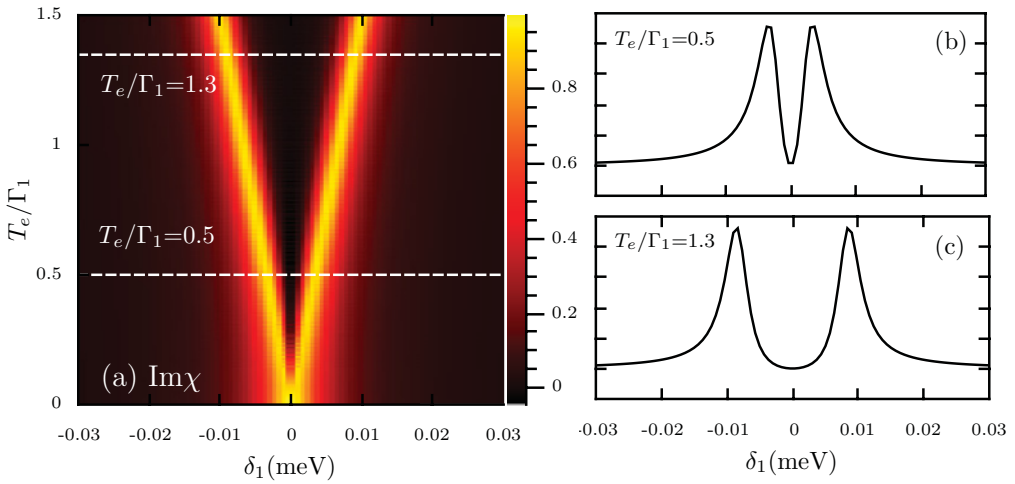

FIG. 5. (Color online) (a) Optical absorption as a function of detuning δ_1 and the ratio T_e/Γ_1 for $\omega_{21} = 0$. In (b) and (c) is shown two different tunneling coupling regimes (white dashed lines).

of optical susceptibility are plotted in Figs. 3(a) and 3(d), respectively. The imaginary part or optical absorption shows the TIT dip at the full resonance condition: $\delta_1 = \omega_{21} = 0$, as shown in Fig. 3(b). For other values of δ_1 and ω_{21}, the position of the absorption minimum follows the condition $\omega_{21} + \delta_1 = 0$. When the electric field is set such that $\omega_{21} \neq 0$, the position of the minimum of absorption occurs for $\delta_1 \neq 0$ with a nonsymmetrical profile, as shown in Fig. 3(c) for $\omega_{21} = -0.01$ meV (red line). This is because the resonance R_b keeps a Lorentzian shape, while the negative resonance R_a produces the displacement of the absorption dip following the condition $\delta_1 + \omega_{21} = 0$. This behavior allows us to control the transparency window with an external electric field. Away from resonance, as shown in Fig. 3(c) for $\omega_{21} = 0.04$ meV (black line), the relative intensity of the negative resonance R_b decreases and the absorption is dominated by the R_b resonance. In this situation, the optical response of the QDM behaves as a typical two-level system, as expected.

The behavior of the real part of the optical susceptibility, Fig. 3(d), shows the same features along the line defined by $\omega_{21} + \delta_1 = 0$. Considering the condition $\omega_{21} = 0$, the real part shows a sharp variation around $\delta_1 = 0$, which represents a large positive derivative in the refractive index, as shown in Fig. 3(e). As we can see from the comparison between the full resonance case and the situation when $\omega_{21} = -0.01$ meV [red line in Fig. 3(f)], the positive derivative position can be controlled by changing the electric field (ω_{21}) and adjusting the laser detuning, such as the condition $\delta_1 + \omega_{21} = 0$ is fulfilled. Again, this effect is related with resonances $R_{a,b}$: the contribution of resonance R_a to the real part of susceptibility is responsible for the positive derivative shown in Fig. 3(e). The contribution of resonance R_b produces a behavior similar to a two-level system and becomes dominant for large values of ω_{21}, as seen for $\omega_{21} = 0.04$ meV in Fig. 3(f) (black line).

In order to compare TIT with ATS behaviors, we show in Fig. 4 the optical susceptibility for $T_e/\Gamma_1 = 1$. We can see in Figs. 4(a) and 4(d) that the two-level behavior of real and imaginary parts of the susceptibility is broken around the condition $\delta_1 + \omega_{21} \sim 0$. The region of zero absorption occurs in the gap between the resonances R_a and R_b. For $\omega_{21} = 0$, as shown in Fig. 4(b), the absorption profile is symmetric about $\delta_1 = 0$ and its shape is defined by the superposition of two identical Lorentzian-like functions. On the other hand, for $\omega_{21} \neq 0$, the symmetry is broken and the components R_a and R_b behave differently. One of the components always keep the Lorentzian-like shape, while the other one becomes narrow and moves out of the center ($\delta_1 = 0$), as we can see in Fig. 4(c) for $\omega_{21} = -0.01$ meV (red line). For even larger values of ω_{21}, the shape of absorption spectrum becomes a single Lorentzian-like function resembling the absorption of a two-level system, which is shown in Fig. 4(c) (black line) for $\omega_{21} = 0.04$ meV. The real part of susceptibility for ATS condition, depicted on Fig. 4(d) for $\omega_{21} = 0$, shows that the positive derivative around $\delta_1 = 0$ is smaller than those obtained for TIT condition. This derivative decreases when ω_{21} increases, as shown in Fig. 4(f) for $\omega_{21} = -0.01$ meV (red line) until the behavior of Reχ is nearly similar to a two-level system, which is shown in Fig. 4(f) for $\omega_{21} = 0.04$ meV (black line).

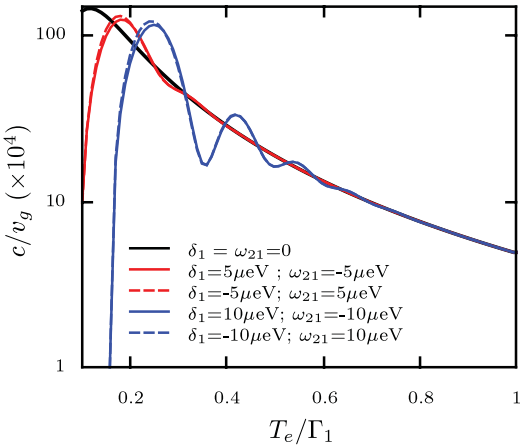

FIG. 6. (Color online) Dependence of the rate c/v_g with the T_e/Γ_1 ratio following the condition $\delta_1 + \omega_{21} = 0$.

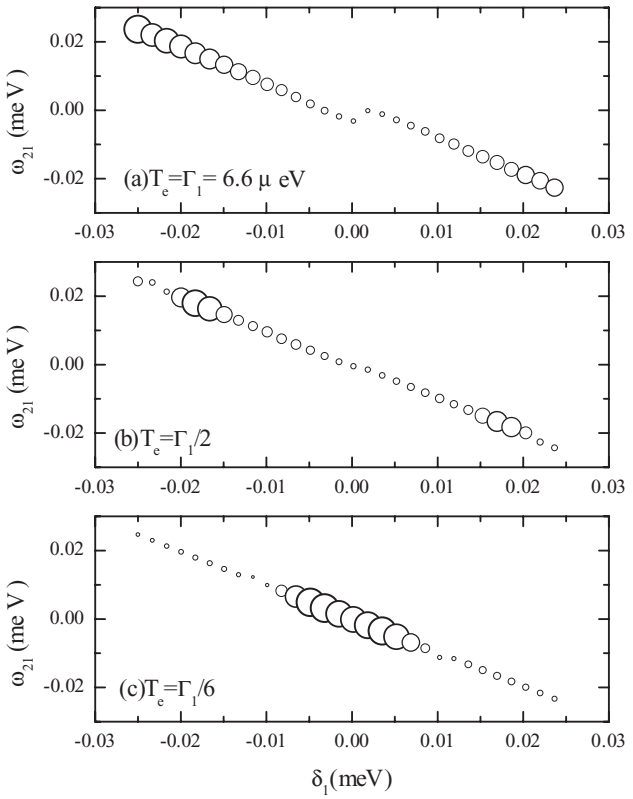

FIG. 7. Variation of the maximum values of c/v_g with δ_1 and ω_{21}. Areas of circles are proportional to c/v_g and the maximum circle area correspond to $c/v_g = 10^5$.

To finish our analysis about the difference between tunneling TIT and ATS regimes for a QDM, we plot in Fig. 5 the imaginary part of susceptibility as a function of both, laser detuning δ_1 and the ratio T_e/Γ_1. We can observe that the width of the zero absorption region (Δ), increases when the ratio T_e/Γ_1 increases. Our numerical analysis shows that for $T_e/\Gamma_1 \gg 1$ (ATS) the absorption gap Δ is proportional to T_e. For $T_e/\Gamma_1 \ll 1$, we establish that $\Delta \propto \sqrt{T_e/\Gamma_1}$.

As discussed ion Sec. II, the light group velocity, given by Eq. (7), is a function of the derivative of the refractive index dn/dw_L. Alternatively, a quantity commonly used to evaluate the variations of group velocity is the ratio c/v_g, which is directly proportional to dn/dw_L. Our calculations of $\mathrm{Re}\chi$ show that there is an appreciable positive variation of the derivative whenever the condition $\delta_1 + \omega_{21} = 0$ is satisfied. Here, we focus our calculations of c/v_g ratio around this particular condition in order to obtain the maximum value of c/v_g or, equivalently, the minimization of the group velocity for a given choice of T_e/Γ_1. In Fig. 6, we plot this quantity as a function of T_e/Γ_1, considering different values of δ_1 and ω_{21}. We note that the maximum value $c/v_g \approx 10^6$ is obtained at full resonance condition ($\delta_1 = \omega_{21} = 0$) when T_e/Γ_1 tends to zero. On the other hand, as expected, the c/v_g ratio decreases rapidly when the T_e/Γ_1 increases. This is a consequence of the dependence of derivative $dn/d\omega_L$ with T_e when the system evolves from TIT to ATS regimes. Out of the full resonance condition, red and blue lines on Fig. 6, the maximum value is obtained for T_e/Γ_1 values that depend on δ_1 and ω_{21}. This behavior does not depend on the sign of the parameters, as can be seen by comparing solid and dashed lines for each choice of δ_1 and ω_{21} values.

These results allow us to say that with an appropriate choice of laser detuning, electric field, and tunneling coupling, we can optimize the slow light phenomena in artificial QDMs. However, the parameter T_e depends on the double quantum dot barrier, and is therefore defined in the growth process of the sample. This situation, makes the tunneling manipulation technically complicated.

In Fig. 7, we show the maximum values of c/v_g ratio as a function of detuning parameters ω_{21} and δ_1 for some fixed values of tunneling T_e. As expected, we observed that the maxima c/v_g rates occur around the condition $\delta_1 + \omega_{21} = 0$. At the ATS condition, depicted in panel (a), we observe that these maximum values are spread out over a wide range of positive and negative values of δ_1 and ω_{21} parameters. As the system evolves to the TIT condition, we observe that the c/v_g maximum ratio are compressed at narrow regions of detuning parameters, panel (b), and when the system reaches the TIT regime, the maximum c/v_g ratio is located around the complete resonance condition $\delta_1 = \omega_{21} \sim 0$. Thus, depending on the value of tunneling, in principle, it is possible to find a regime of detuning parameters that maximize c/v_g or, equivalently, minimize the light group velocity.

IV. CONCLUSIONS

In this work, we explore the optical properties of QDMs, by considering a direct and indirect excitonic states coupled by tunneling. A laser field promotes an electron from valence to conduction band, creating the direct exciton, and a gate electric field is used to manipulate the levels detuning. Our numerical solution of the Liouville-von Neumman-Lindblad equation, Eq. (2), shows that optical susceptibility has two different behaviors, which depend on the ratio between the tunneling coupling T_e and the decoherence parameter Γ_1; for values below the threshold given by $T_e/\Gamma_1 = 0.5$, the system shows TIT. Above this value, the physical behavior corresponds to ATS. We showed that in the TIT regime, the optical absorption exhibits its characteristic transparency window when laser is in resonance with the frequency of the direct exciton transition. With an external electric field, we have an additional control parameter (the detuning ω_{21}), which opens the possibility to shift and optimize the transparency window. This property could be used to construct a high-resolution light filter. Additionally, we have mapped the behavior of the light group velocity as a function of detunings δ_1 and ω_{21} for different values of the ratio T_e/Γ_1. We found that light group velocity could be reduced by a factor of 10^6 in QDMs.

ACKNOWLEDGMENTS

This work was supported by CAPES, FAPEMIG, CNPq, and the Brazilian National Institutes of Science and Technology for Quantum Information (INCT-IQ) and for Semiconductor Nanodevices (INCT-DISSE).

[1] M. Fleischhauer, A. Imamoglu, and J. P. Marangos, Rev. Mod. Phys. **77**, 633 (2005).
[2] X. Xu, B. Sun, P. R. Berman, D. G. Steel, A. S. Bracker, D. Gammon, and L. J. Sham, Science **317**, 929 (2007).
[3] J. Berney, M. T. Portella-Oberli, and B. Deveaud, Phys. Rev. B **77**, 121301(R) (2008).
[4] H. Gotoh, H. Kamada, T. Saitoh, H. Ando, and J. Temmyo, Phys. Rev. B **71**, 195334 (2005).
[5] S. Marcinkevicius, A. Gushterov, and J. P. Reithmaier, Appl. Phys. Lett. **92**, 041113 (2008).
[6] M. Phillips and H. Wang, Phys. Rev. Lett. **89**, 186401 (2002).
[7] K.-M. C. Fu, C. Santori, C. Stanley, M. C. Holland, and Y. Yamamoto, Phys. Rev. Lett. **95**, 187405 (2005).
[8] D. Brunner, B. D. Gerardot, P. A. Dalgarno, G. Wüst, K. Karrai, N. G. Stoltz, P. M. Petroff, and R. J. Warburton, Science **325**, 70 (2009).
[9] E. A. Stinaff, M. Scheibner, A. S. Bracker, I. V. Ponomarev, V. L. Korenev, M. E. Ware, M. F. Doty, T. L. Reinecke, and D. Gammon, Science **311**, 636 (2006).
[10] H. S. Borges, L. Sanz, J. M. Villas-Bôas, and A. M. Alcalde, Phys. Rev. B **81**, 075322 (2010).
[11] M. Bayer, P. Hawrylak, K. Hinzer, S. Fafard, M. Korkusinski, Z. R. Wasilewski, O. Stern, and A. Forchel, Science **291**, 451 (2001).
[12] D. Kim, S. G. Carter, A. Greilich, A. S. Bracker, and D. Gammon, Nat. Phys. **7**, 223 (2010).
[13] C.-H. Yuan and K.-D. Zhu, Appl. Phys. Lett. **89**, 052115 (2006).
[14] J. E. Rolon and S. E. Ulloa, Phys. Rev. B **82**, 115307 (2010).
[15] A. S. Bracker, M. Scheibner, M. F. Doty, E. A. Stinaff, I. V. Ponomarev, J. C. Kim, L. J. Whitman, T. L. Reinecke, and D. Gammon, Appl. Phys. Lett. **89**, 233110 (2006).
[16] J. M. Villas-Boâs, A. O. Govorov, and S. E. Ulloa, Phys. Rev. B **69**, 125342 (2004).
[17] A. J. Ramsay, A. V. Gopal, E. M. Gauger, A. Nazir, B. W. Lovett, A. M. Fox, and M. S. Skolnick, Phys. Rev. Lett. **104**, 017402 (2010).
[18] P. Borri, W. Langbein, U. Woggon, M. Schwab, M. Bayer, S. Fafard, Z. Wasilewski, and P. Hawrylak, Phys. Rev. Lett. **91**, 267401 (2003).
[19] H. Kamada, H. Gotoh, J. Temmyo, T. Takagahara, and H. Ando, Phys. Rev. Lett. **87**, 246401 (2001).
[20] N. H. Bonadeo, J. Erland, D. Gammon, D. Park, D. S. Katzer, and D. G. Steel, Science **282**, 1473 (1998).
[21] P. Chen, C. Piermarocchi, and L. J. Sham, Phys. Rev. Lett. **87**, 067401 (2001).
[22] T. Calarco, A. Datta, P. Fedichev, E. Pazy, and P. Zoller, Phys. Rev. A **68**, 012310 (2003).
[23] G. Ortner, M. Schwab, P. Borri, W. Langbein, U. Woggon, M. Bayer, S. Fafard, Z. Wasilewski, P. Hawrylak, Y. B. Lyanda-Geller, T. L. Reinecke, and A. Forchel, Physica E **25**, 256 (2004).
[24] C. Bardot, M. Schwab, M. Bayer, S. Fafard, Z. Wasilewski, and P. Hawrylak, Phys. Rev. B **72**, 035314 (2005).
[25] L. V. Butov, A. Zrenner, G. Abstreiter, G. Bohm, and G. Weimann, Phys. Rev. Lett. **73**, 304 (1994).
[26] A. Tackeuchi, T. Kuroda, K. Mase, Y. Nakata, and N. Yokoyama, Phys. Rev. B **62**, 1568 (2000).
[27] C. Emary and L. J. Sham, Phys. Rev. B **75**, 125317 (2007).
[28] J. Kim, S. L. Chuang, P. C. Ku, and C. J. Chang-Hasnain, J. Phys: Condens. Matter **16**, S3727 (2004).
[29] T. Y. Abi-Salloum, Phys. Rev. A **81**, 053836 (2010).